THE JOURNAL OF PHYSICAL CHEMISTRY A
A JOURNAL OF THE AMERICAN CHEMICAL SOCIETY

pubs.acs.org/JPCA

Article

Interplay of Near-Zero-Field Dephasing, Rephasing, and Relaxation Dynamics and [1-^{13}C]Pyruvate Polarization Transfer Efficiency in Pulsed SABRE-SHEATH

Shiraz Nantogma, Shannon L. Eriksson, Isaiah Adelabu, Iuliia Mandzhieva, Austin Browning, Patrick TomHon, Warren S. Warren, Thomas Theis, Boyd M. Goodson, and Eduard Y. Chekmenev*

Cite This: https://doi.org/10.1021/acs.jpca.2c07150

Read Online

ACCESS | Metrics & More | Article Recommendations

ABSTRACT: Hyperpolarized [1-^{13}C]pyruvate is a revolutionary molecular probe enabling ultrafast metabolic MRI scans in 1 min. This technology is now under evaluation in over 30 clinical trials, which employ dissolution Dynamic Nuclear Polarization (d-DNP) to prepare a batch of the contrast agent; however, d-DNP technology is slow and expensive. The emerging SABRE-SHEATH hyperpolarization technique enables fast (under 1 min) and robust production of hyperpolarized [1-^{13}C]pyruvate via simultaneous chemical exchange of parahydrogen and pyruvate on IrIMes hexacoordinate complexes. Here, we study the application of microtesla pulses to investigate their effect on C-13 polarization efficiency, compared to that of conventional SABRE-SHEATH employing a static field (~0.4 μT), to provide the matching conditions of polarization transfer from parahydrogen-derived hydrides to the ^{13}C-1 nucleus. Our results demonstrate that using square-microtesla pulses with optimized parameters can produce ^{13}C-1 polarization levels of up to 14.8% (when detected, averaging over all resonances), corresponding to signal enhancement by over 122,000-fold at the clinically relevant field of 1.4 T. We anticipate that our results can be directly translated to other structurally similar biomolecules such as [1-^{13}C]α-ketoglutarate and [1-^{13}C]α-ketoisocaproate. Moreover, other more advanced pulse shapes can potentially further boost heteronuclear polarization attainable via pulsed SABRE-SHEATH.

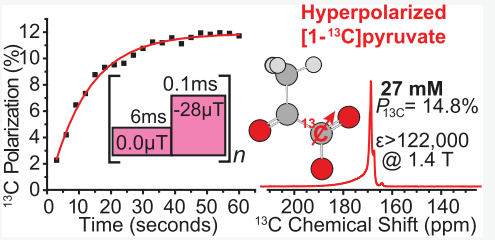

INTRODUCTION

NMR hyperpolarization increases nuclear spin polarization above thermal levels by 4−6 orders of magnitude, with corresponding gains in the detected signal.[1−6] Hyperpolarized (HP) MRI has emerged as a promising alternative to Positron Emission Tomography (PET) tracers for real-time metabolic imaging because low-concentration metabolites such as pyruvate can be mapped *in vivo*.[7−9] Moreover, detection of ^{13}C-hyperpolarized nuclei enables imaging without a tissue background signal.[10] Unlike PET, HP MRI employs no ionizing radiation.[11] Moreover, HP MRI scans can be completed in 1 min, offering unprecedented exam speed.[11] HP [1-^{13}C]pyruvate has emerged as the key HP contrast agent for probing anaerobic glycolysis, a central metabolic pathway frequently upregulated in cancers and other metabolically challenging diseases.[3,12,13] The pyruvate ^{13}C-1 nucleus offers a relatively long HP state lifetime *in vivo* (T_1 of ~1 min) and excellent chemical shift dispersion of downstream metabolites ([1-^{13}C]lactate, ^{13}C-bicarbonate, and [1-^{13}C]alanine), enabling their simultaneous mapping via spectroscopic MRI.[3,12] HP [1-^{13}C]pyruvate can potentially revolutionize molecular imaging in the future.[3,12] This leading HP contrast agent is now under evaluation in over 30 clinical trials according to clinicaltrials.gov.

HP [1-^{13}C]pyruvate is currently produced at clinical scales via dissolution Dynamic Nuclear Polarization (d-DNP), which employs cryogenic temperatures, high magnetic fields, and high-power microwave irradiation.[14,15] This technology is expensive: a clinical-scale device costs over $2 million, and it also requires expensive cryogens for operation. More importantly, 5 T SpinLab devices need approximately 1 h to produce a clinical dose of HP [1-^{13}C]pyruvate with ^{13}C polarization (P_{13C}) of 35−40% with a typical failure rate of 13%.[16] As a result, slow and expensive hyperpolarization production limits the biomedical translation of ultrafast HP [1-^{13}C]pyruvate MRI. Therefore, faster, more robust, and more affordable approaches are needed to accelerate the accessibility of HP [1-^{13}C]pyruvate to accelerate preclinical development and for ultimate widespread clinical use.

Received: October 11, 2022
Revised: November 4, 2022

In 2009, Duckett and co-workers pioneered Signal Amplification by Reversible Exchange (SABRE), a hyperpolarization technique that relies on a simultaneous exchange of parahydrogen (pH_2)[17] and to-be-hyperpolarized substrates on metal complexes.[18] The spin order of pH_2 is spontaneously transferred to the substrate during the exchange without chemical modification of the substrate.[19] In 2015, we demonstrated SABRE in SHield Enables Alignment Transfer to Heteronuclei (SABRE-SHEATH), including polarization enhancement of ^{15}N[20,21] and ^{13}C,[22] which have substantial biomedical importance. In 2019−2020, Duckett and co-workers have demonstrated the feasibility of [1-^{13}C]pyruvate hyperpolarization via SABRE-SHEATH.[23,24] Moreover, we have recently reported on refining this approach to substantially boost the attainable P_{13C} of [1-^{13}C]pyruvate.[25−27] A key innovation to enable [1-^{13}C]pyruvate exchange on the time scale suitable for polarization transfer from pH_2 to the ^{13}C-1 nucleus is the use of DMSO to co-ligate the iridium hexacoordinate complex (Figure 1a).[23,24] A series of other recent innovations including temperature-cycling and the use of water enabled P_{13C} values of [1-^{13}C]pyruvate to be greatly increased from 1.85%[23,24] to 13%,[25,26] enabling SABRE-hyperpolarized pyruvate to be potentially usable for *in vivo* studies.[28] Unlike d-DNP, SABRE-SHEATH is highly scalable, rapid (1 min), and relatively inexpensive (the device costs approximately $20k)[29] and thus is a potentially game-changing technology to empower the biomedical community with an inexpensive source of the HP [1-^{13}C]pyruvate contrast agent on demand.

The hyperpolarization dynamics of the SABRE process is complex,[30] and the selectivity of polarization transfer from pH_2−derived protons to an X nucleus (*e.g.*, ^{13}C) can be potentially improved via the application of microtesla field pulses.[31,32] Recent theoretical and experimental studies have demonstrated that P_{15N} can indeed be improved via pulsed SABRE-SHEATH[33] with polarization gains of up to ∼3-fold,[33] resulting in P_{15N} of ∼10% in [^{15}N]acetonitrile.[34]

Here, we demonstrate that when microtesla field pulses are applied during SABRE-SHEATH, it becomes possible to obtain P_{13C} of [1-^{13}C]pyruvate up to ∼14.8% (Figure 1b), corresponding to over 122,000-fold signal enhancement at the clinically relevant magnetic field of 1.4 T (a spectrum of thermally polarized neat [1-^{13}C]acetic acid employed as a signal reference is shown in Figure 1c).

MATERIALS AND METHODS

Sample Preparation. Each sample was prepared by creating a stock solution of 30 mM of [1-^{13}C]pyruvate mixed with 20 or 40 mM of DMSO (dried over molecular sieves) in 2.0 mL of CD_3OD. Six hundred microliter of this stock solution was measured into a 1.5 mL Eppendorf tube containing 2.3 mg of SABRE precatalyst (IrCl(COD)(IMes),[35,36] **1**) and 60 μL of 10% HPLC-grade water in CD_3OD. This procedure results in a precatalyst concentration of 6 mM, a [1-^{13}C]pyruvate concentration of 27 mM, a DMSO concentration of 18 or 36 mM, and an H_2O concentration of 0.5 M. Each sample was then transferred into a medium-wall NMR tube and purged with ultrahigh purity Argon gas for 2 min and capped. The sample was then taken to the polarizer setup for activation. All experiments were performed using a cold-water bath with temperature of 10 °C.

Sample Activation. Each sample was activated by bubbling p-H_2 gas (>98% para- state[37]) through the sample

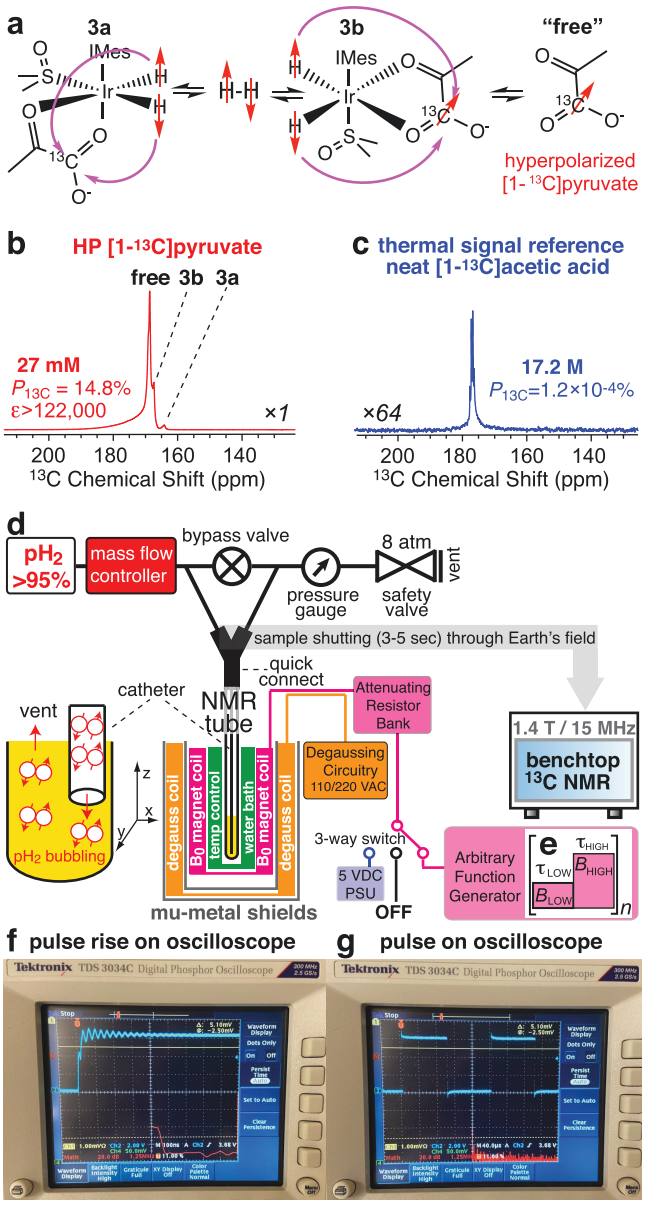

Figure 1. (a) Schematic of simultaneous chemical exchange of pH_2 and [1-^{13}C]pyruvate on activated IrIMes catalyst complexes **3a** and **3b**[23] to yield "free" HP [1-^{13}C]pyruvate. (b) ^{13}C NMR spectrum of 27 mM HP sodium [1-^{13}C]pyruvate prepared via pulsed SABRE-SHEATH (p-H_2 flow of 120 sccm at 9.2 atm; τ_{LOW} = 6 ms; τ_{HIGH} = 0.1 ms; B_{LOW} < 40 nT; B_{HIGH} = −28 μT) using 6 mM IrCl(COD)(IMes) precatalyst, 18 mM DMSO, 0.5 M water in CD_3OD at 10 °C; total ^{13}C polarization values are reported via signal integration over the three peaks. (c) Corresponding ^{13}C spectrum of signal reference compound (neat [1-^{13}C]acetic acid). (d) Schematic of the experimental setup (B_0 field inside the shields is applied along z-direction; note that residual *x*−*y* static magnetic fields may exist in the shields). (e) Schematic of SABRE-SHEATH pulse sequence. (f) Photograph of an oscilloscope screen showing a close-up of the magnetic field pulse rise of less than 0.1 μs. (g) Corresponding photograph of the magnetic field pulse sequence.

for 20 min inside the magnetic shield of the polarizer. This activation step is performed after purging the gas manifold of the hyperpolarizer with p-H_2 gas for at least 5 min to remove any trapped oxygen-containing air. The precatalyst **1** activation leads to formation of complexes **1**, **3a**, and **3b** as described previously, Scheme 1.[23−26] Only complex **3b** is SABRE active,

https://doi.org/10.1021/acs.jpca.2c07150
J. Phys. Chem. A XXXX, XXX, XXX−XXX

that is, leading to formation of free HP [1-^{13}C]pyruvate, Figure 1a.

Scheme 1. Schematic of SABRE Precatalyst Activation to Form Complexes 2, 3a, and 3b[a]

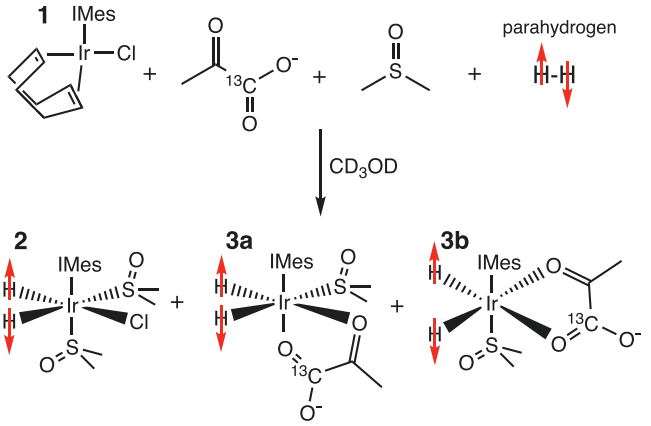

[a]Complex **2** is not SABRE-SHEATH active. The scheme is adopted from ref 25. The precatalyst complex **1** was synthesized as described previously.[35,36,38] Reproduced with permission from ref 25. Copyright 2022 Wiley.

SABRE-SHEATH Hyperpolarizer. Briefly, as described previously,[25] the integrated setup consists of a two-layered mu-metal shield (ZG-206, Magnetic Shield, Corp., Bensenville, IL) to attenuate the Earth's magnetic field to less than 40 nT residual field.[39] The field inside the shield was created via a compensated solenoid coil using either a DC power supply (for conventional SABRE-SHEATH, at fixed field of −0.42 μT with 90% homogeneity over its 7″ length) or via the output signal of an arbitrary function generator (AFG1062, Tektronix, Beaverton). The field was monitored by a 3-axis fluxgate magnetometer (Mag-03, Bartington, Witney, U.K.). The activated sample (in a 5 mm NMR tube) was bubbled with pH_2 (~8 atm total pressure (unless otherwise noted) and 70 standard cubic centimeters per minute (sccm) unless noted otherwise) at an optimized temperature of 10 °C,[25]Figure 1c, either using the static −0.42 μT field or microtesla pulses as shown in Figure 1d. After SABRE-SHEATH hyperpolarization was completed, the pH_2 bubbling was ceased, and the sample was manually shuttled to a 1.4 T benchtop NMR spectrometer: either a SpinSolve Carbon 60 (Magritek) or an NMR Pro60 (Nanalysis), Figure 1. The delay between p-H_2 flow cessation and acquisition of an enhanced ^{13}C NMR spectrum (without proton decoupling) was approximately 3−5 s.

SABRE-SHEATH Hyperpolarization at a Static Field of −0.42 μT. The sample was placed at the center of the shield with a static magnetic field of −0.42 μT (created by an electromagnet placed in the degaussed mu-metal shield; the DC current was attenuated via a resistor bank to achieve the desired field[39] and the field was verified by a fluxgate magnetometer; note the field inside the shield is negative with respect to the detecting 1.4 T magnet) and bubbled with p-H_2 for ~30 s at a flow rate of 70 sccm and total p-H_2 pressure of 8 bar (unless noted otherwise). The sample was then quickly transferred into a 1.4 T benchtop NMR spectrometer for detection as described above.

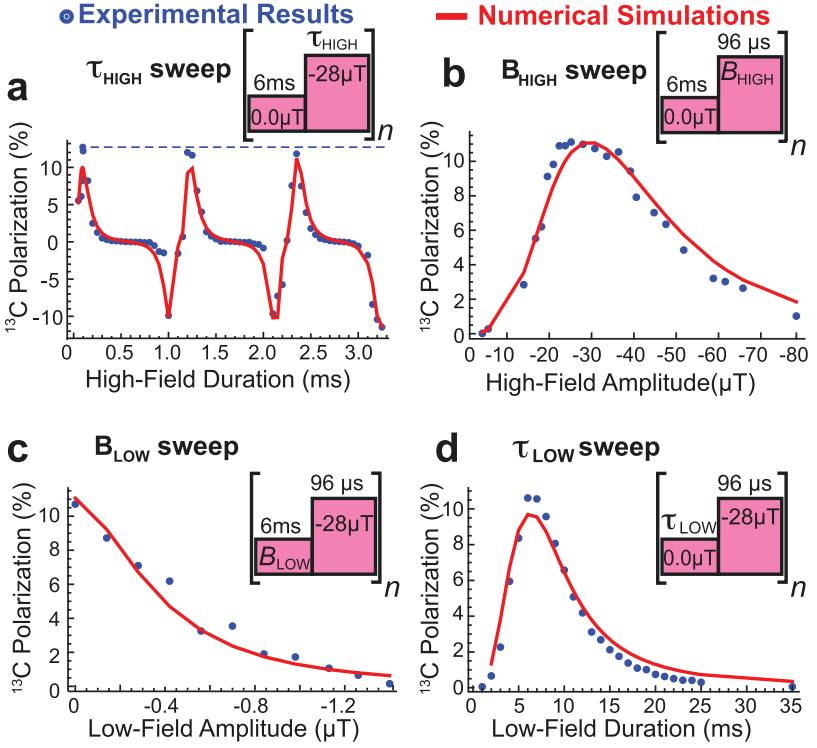

Figure 2. Pulsed SABRE-SHEATH: dependence of ^{13}C-1 polarization of [1-^{13}C]pyruvate on the high-field pulse duration, τ_{HIGH} (a); the high-field pulse amplitude, B_{HIGH} (b); the low-field pulse amplitude, B_{LOW} (c); and the low-field pulse duration, τ_{LOW} (d). All experiments were performed with ~27 mM [1-^{13}C]pyruvate, 6 mM IrCl(COD)(IMes) precatalyst, 18 mM DMSO, and 0.5 M water in CD_3OD at 10 °C. The blue dashed line in display a is added to guide the eye.

https://doi.org/10.1021/acs.jpca.2c07150
J. Phys. Chem. A XXXX, XXX, XXX−XXX

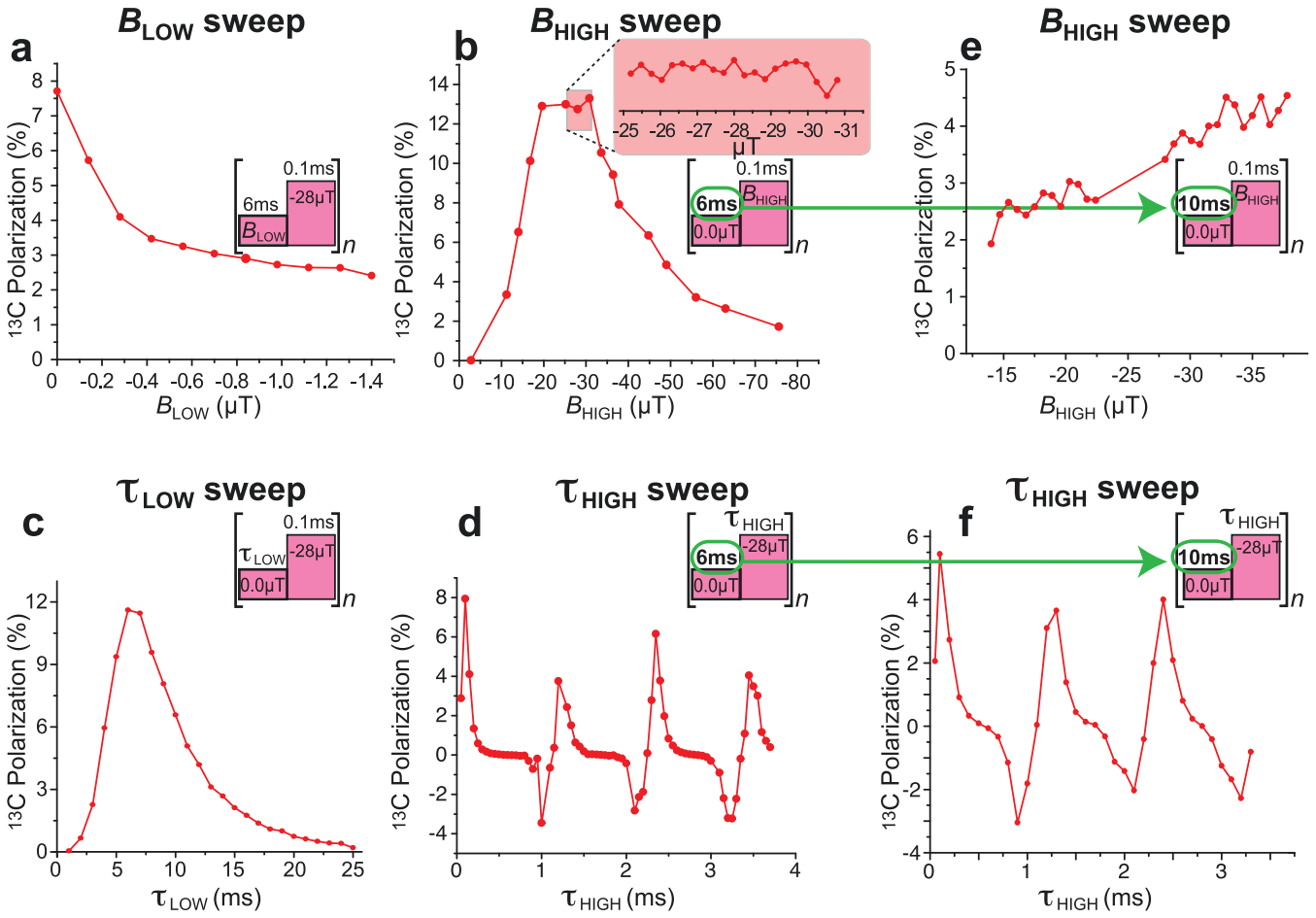

Figure 3. Pulsed SABRE-SHEATH: dependence of ^{13}C-1 polarization of [1-^{13}C]pyruvate on the low-field amplitude, B_{LOW} (a); the high-field amplitude, B_{HIGH} (b); the duration of the low-field pulse duration, τ_{LOW} (c); and the duration of the high-field pulse duration, τ_{HIGH} (d). Additional displays (e) and (f) are added as illustrative examples of performing field and duration sweeps at sub-optimal sets of experimental parameters. All experiments were performed with ~27 mM [1-^{13}C]pyruvate, 6 mM IrCl(COD)(IMes) precatalyst, 18 mM DMSO, and 0.5 M water in CD_3OD at +10 °C. Lines between the data points are added to guide the eye.

Pulsed SABRE-SHEATH Hyperpolarization. Pulse sequence parameters (schematically shown in Figure 1e) were set on an arbitrary function generator (AFG1062, Tektronix, Beaverton) by creating a square pulse with an amplitude of 2.5 V and zero-offset of −14 to −18 mV (to ensure that the field is set to less than 40 nT (the detection limit of our magnetometer)), a period of 4 s, and a duty cycle of 2 s. The pulse rise and duration were verified via oscilloscope, Figure 1f,g, respectively. This approach allows us to measure the exact low-field and high-field amplitudes using a fluxgate magnetometer and to adjust the current (and by extension, the magnetic field of the coil) using a resistor bank before we proceed with the actual pulse (note that setting the field strength parameters of the sequence with high-frequency oscillations would render an average value detected by the magnetometer, which is not what we want). Once the high- and low-field amplitudes were confirmed, the low-field and high-field durations were set on the waveform generator and turned off. Hyperpolarization experiments were then started by turning on the waveform generator and p-H_2 bubbling valve at the same time. The p-H_2 bubbling was stopped after 30 s and allowed to settle for a second before the sample was transferred to the NMR spectrometer for detection as detailed above. Examples of pulsed SABRE-SHEATH studies are shown in Figure 2a−d.

^{13}C NMR Data Acquisition for ^{13}C Polarization Build-Up Measurements. The [1-^{13}C] polarization build-up curves (*e.g.*, Figure 3a) were obtained by varying the duration of p-H_2 bubbling of the sample placed inside the shield—one data point was obtained from each experiment with variable duration of p-H_2 bubbling. All other experimental parameters were kept the same.

^{13}C NMR Data Acquisition for ^{13}C Polarization In-Shield T_1 Decay Measurements at −0.42 μT. The ^{13}C polarization was allowed to build for 30 s during p-H_2 bubbling. Next, the p-H_2 flow was stopped by opening the bypass valve, Figure 1d. Next, the sample was allowed to stay in the shield for ^{13}C polarization decay for a given period prior to rapid transfer to the high field (1.4 T) for detection, for example, Figure 3b. Thus, the data was collected by acquiring one data point per each experiment. All other experimental parameters were kept the same. All data points before t = 6 s were excluded (from the data fitting) to eliminate any contribution from residual polarization build-up inside the shield due to residual p-H_2.

^{13}C NMR Data Acquisition for ^{13}C Polarization In-Shield T_1 Decay Measurements in Pulsed-SABRE-SHEATH. These studies were performed by bubbling p-H_2 in the shield for 30 s, while the pulse was running and then varying the time the sample spent in the shield after cessation

https://doi.org/10.1021/acs.jpca.2c07150
J. Phys. Chem. A XXXX, XXX, XXX−XXX

of p-H_2 bubbling before detection—one data point was obtained from each experiment. All other experimental parameters were kept the same. All data points before t = 6 s (from the data fitting) were excluded to eliminate any contribution from polarization build-up inside the shield due to residual p-H_2.

^{13}C NMR Data Acquisition for ^{13}C Polarization T_1 Decay in the Earth's Field (*ca.* 50 μT). These studies were performed by p-H_2 bubbling in the shield for 30 s and then quickly shuttling the sample out of the shield and into the Earth's field and then varying the time the sample has spent in the Earth's field before detection at 1.4 T. One data point was obtained from each experiment. All other experimental parameters were kept the same. All data points before t = 6 s were excluded to eliminate any contribution from polarization build-up due to residual p-H_2.

^{13}C NMR Data Acquisition for ^{13}C Polarization T_1 Decay in 1.4 T Field. The studies were performed by p-H_2 bubbling in the shield for 30 s. The p-H_2 flow was stopped, and the sample was transferred to the 1.4 T NMR spectrometer. Then, we varied the duration of time that the HP sample spent in the spectrometer before NMR detection—one data point was obtained from each experiment. All other experimental parameters were kept the same. All data points before t = 6 s (from the data fitting) were excluded to eliminate any contribution from polarization build-up due to residual p-H_2.

Computation of ^{13}C Polarization Enhancement and Polarization Values. ^{13}C NMR signals from [1-^{13}C]pyruvate (concentration, C_{HP} = 0.027 M) were recorded using single-scan acquisitions using a 1.4 T benchtop NMR spectrometer as described above. The HP spectra were recorded from samples placed in medium-wall NMR tubes with a 1/16″ OD Teflon catheter placed inside. The obtained HP signal (S_{HP}) was compared to a thermally polarized signal reference sample (neat [1-^{13}C]acetic acid, C_{REF} = 17.5 M, Figure 3c) placed inside a regular-wall NMR tube. ^{13}C signal enhancements (ε_{13C}) were computed using eq 1 as described previously[25]

$$\varepsilon_{13C} = \frac{S_{HP}}{S_{REF}} \times \frac{C_{REF}}{C_{HP}} \times \frac{A_{REF}}{A_{HP}} = \frac{S_{HP}}{S_{REF}} \times \frac{C_{REF}}{C_{HP}} \times 1.705 \quad (1)$$

where A_{REF} and A_{HP} are effective cross-sections of reference and HP samples in the regular-wall and medium-wall NMR tubes, respectively. The ratio (A_{REF}/A_{HP}) was determined experimentally for both NMR spectrometers employed and was found to be 1.705 and was used in eq 1. The P_{13C} value was computed according to eq 2

$$P_{13C} = \varepsilon_{13C} \times P_{therm} \quad (2)$$

where P_{therm} (1.20×10^{-4}%) is the ^{13}C thermal polarization level at 1.4 T and 298 K.

An example of ^{13}C signal enhancement and polarization calculations for the spectrum shown in Figure 1b is provided below

$$\varepsilon_{13C} = \frac{10849}{97.77} \times \frac{17.5}{0.0270} \times 1.705 = 1.22 \times 10^5$$

$$P_{13C} = 1.22 \times 10^5 \times 1.20 \times 10^{-4}\% = 14.8\%$$

Numerical Simulations. All simulations were run using a physically accurate numerical simulation method introduced by the Warren lab in 2020.[33] The modeled spin system was simplified extensively (Scheme 2) because many of the exchange and coupling parameters are as yet unknown. The imposed simplifications are as follows: (1) the methyl protons are truncated out of both the free and bound spin systems; (2) only the polarization transfer complex **3b** is simulated here; (3) the J coupling network has not been fully determined for this configuration, so the parameters used were not experimentally measured, but rather assumed or fit to the data; (4) the target ligand dissociation rate and hydride association rate have not been determined in this complex in the published literature. The hydride association rate ($k_{a,H}$) was fixed at 0.2 s^{-1} because the impact of this rate on the fine structure of the plots is minimal. The ligand dissociation rate was fit to the data ($k_{d,N}$).

Scheme 2. Schematic of the Three-Spin System and Relevant Parameters Employed in the Numerical Simulations

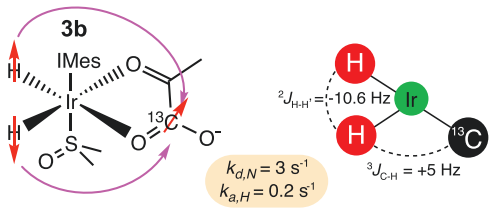

All parameters used in the simulations were either defined ($^2J_{H-H'}$ = −10 Hz, $k_{a,H}$ = 0.2 s^{-1}), set to the experimental values (magnetic field sequence, relative concentrations of ligand and catalyst), or varied to fit the experimental data ($^3J_{C-H}$,$k_{d,N}$).

The experimental results presented in Figures 2a–d and 4 were simulated, and the $^3J_{C-H}$ and $k_{d,N}$ values were determined by minimization of the RMSD between the experimental and numerical results.

RESULTS AND DISCUSSION

We used this simple experimental apparatus to investigate the application of pulsed SABRE-SHEATH sequences on ^{13}C-pyruvate complexes. Starting with a zero-field, high-field pulse sequence, varying the duration of the high-field pulse, τ_{HIGH},

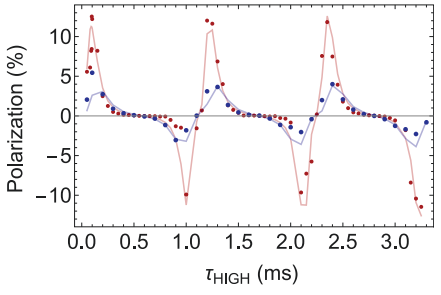

Figure 4. Fitting exchange rates from pulsed SABRE-SHEATH τ_{HIGH} sweeps. The red data set (points) has pulse parameters τ_{LOW} = 6 ms, B_{LOW} = 0 μT, and B_{HIGH} = −28 μT, and the blue has pulse parameters τ_{LOW} = 10 ms, B_{LOW} = 0 μT, and B_{HIGH} = −28 μT. All experiments were performed with ~27 mM [1-^{13}C]pyruvate, 6 mM IrCl(COD)-(IMes) precatalyst, 18 mM DMSO, and 0.5 M water in CD_3OD at 10 °C. Numerical simulations (solid lines) used experimental parameters and spin coupling network (see Methods section) and fit to a $k_{d,N}$ = 4 s^{-1}. The positions of the extrema in the τ_{HIGH} sweep are highly dependent on both the exchange rate and τ_{LOW}. Experimentally sweeping through τ_{HIGH} at a second τ_{LOW} duration (τ_{LOW} = 10 ms) demonstrates this shift.

https://doi.org/10.1021/acs.jpca.2c07150
J. Phys. Chem. A XXXX, XXX, XXX−XXX

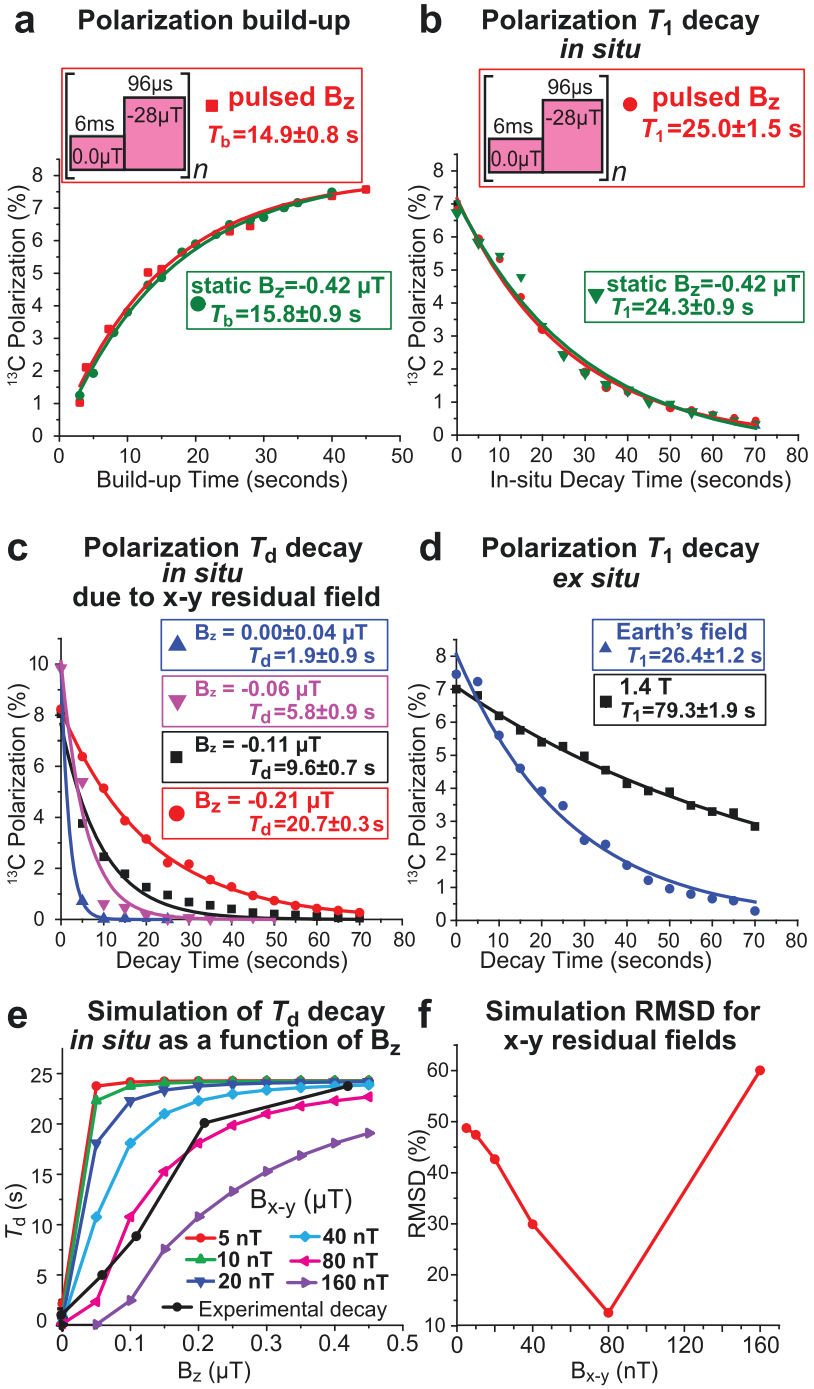

Figure 5. (a) ^{13}C-1 polarization build-up of [1-^{13}C]pyruvate via conventional SABRE-SHEATH (−0.42 μT static field) and pulsed SABRE-SHEATH using (τ_{LOW} = 6 ms; τ_{HIGH}=96 μs; B_{LOW} < 40 nT, B_{HIGH} = −28 μT). (b) ^{13}C T_1 polarization decay of [1-^{13}C]pyruvate at −0.42 μT static field and during application of SABRE-SHEATH pulses. (c) ^{13}C polarization decay of [1-^{13}C]pyruvate due to polarization dephasing associated with the shields' residual magnetization in the $x-y$ plane for four representative magnetic fields of interest applied along the shield's z-direction (see Figure 1d). (d) ^{13}C T_1 polarization decay of [1-^{13}C]pyruvate at the Earth's field and 1.4 T. All experiments were performed with ∼27 mM [1-^{13}C]pyruvate, 6 mM IrCl(COD)(IMes) precatalyst, 18 mM DMSO, and 0.5 M water in CD_3OD at 10 °C. (e) simulations of T_d decay due to $x-y$ in-situ field inhomogeneities as a function of the applied magnetic field B_z; (f) corresponding values of root-mean-square deviation (RMSD) between simulations and experimental results.

results in similar oscillatory behavior in qualitative agreement with previous ^{15}N pulsed SABRE-SHEATH studies.[33,34] The polarization periodically shows sharp resonance conditions centered at specific rotations about the resonance frequency difference, $\Delta\omega_{CH}$, between $\hat{I}_1$ and $\hat{S}$. The polarization transfer minima and maxima are centered about pulse durations τ_{HIGH} that induce an angular rotation $\theta_{HIGH} = 2\cdot\pi\cdot n$, which occurs under pulse conditions that satisfy $\theta_{HIGH} = \tau_{HIGH}\cdot(\omega_H - \omega_C) = 2\cdot\pi\cdot B_{HIGH}\cdot\tau_{HIGH}\cdot(\gamma_H - \gamma_C) = 2\cdot\pi\cdot n$. θ_{HIGH} corresponds to the angular separation between the $\hat{I}_1$ and $\hat{S}$ vectors due to the resonance frequency difference between the carbon-13 and hydride nuclei in the applied field. The transverse components of these vectors will rotate relative to one another at the difference between the precession frequencies of the two

https://doi.org/10.1021/acs.jpca.2c07150
J. Phys. Chem. A XXXX, XXX, XXX−XXX

nuclei. Over a certain time period τ, this angular difference θ_{HIGH} would then be equal to the frequency difference multiplied by the duration that this rotation is occurring: $\theta_{HIGH} = 2\pi(\omega_H - \omega_C)\ \tau_{HIGH} = 2\pi B_{HIGH}\tau_{HIGH}\ (\gamma_H - \gamma_C)$. The extra 2π coefficient is present to ensure the angle is in radians for clarity. This angle is useful in understanding the action of the pulse sequence. Unfortunately, contrary to previous reports, polarization transfer does not improve under larger values of θ in this system as seen by the relatively similar magnitude of the subsequent maxima (versus otherwise expected increase) in Figure 2a. Rather nonintuitively, the benefit of the pulsed SABRE-SHEATH sequences would come from the attenuation of the J coupling between the hydrides and the target nucleus (*e.g.*, $^2J_{H-N}$ between the hydrides and the spin-spin-coupled ^{15}N nucleus in the case of ^{15}N pulsed SABRE-SHEATH[33,34]) or $^3J_{C-H}$ in the case of [1-^{13}C]pyruvate studied here, Scheme 2. The J coupling drives the oscillation of population between the initialized state with singlet spin order on parahydrogen-derived hydrides and a target state with magnetization on the target nucleus. With a large J coupling, this oscillates rapidly and some of the spin order can be returned to the initial state by "back-pumping" before the ligand exchanges at a rate $k_{d,L}$. Reduction of this coupling allows for efficient population transfer into the target state with a reduction of this "back-pumping" effect.

For a spin system like the dominant polarization transfer complexes in [1-^{13}C]pyruvate solutions, the assumed $^3J_{C-H}$ is already small (≈5 Hz) and on the order of the exchange rate calculated for this complex, and so, further effective attenuation of this coupling does not result in meaningful improvements in the polarization transfer.

The optimal τ_{HIGH} from this sweep corresponds to the condition where the time-weighted average of the applied field is equivalent to the optimal continuous field condition. Additional sweeps through the other three parameters in the pulse sequence (B_{HIGH}, B_{LOW}, and τ_{LOW}) shown in Figure 2b–d bear this out. Each parameter is optimized at the condition where the effective field over the course of the pulse sequence is equal to the continuous field optimum. This behavior is in good agreement with numerical simulations shown by the solid red lines overlaying the experimental data (shown by blue circles) in Figure 2a–d.

In fact, this agreement between experimental data and numerical simulations allows for an initial estimate of the ligand exchange rate and J_{CH} coupling for pyruvate bound to the complex **3b**. Using physically accurate numerical simulations of SABRE spin systems in the setting of exchange, we see clear agreement between theoretical predictions and experimental results. By fitting the experimental data in Figure 2a–d with simulation across a range of $k_{d,N}$ and J_{CH}, unreported values to date, we were able to do a preliminary determination of these parameters. The pyruvate exchange rate ($k_{d,N}$) was ∼4 s^{-1}, and the J_{CH} coupling was +5 Hz.

It should be noted that if the experiment is performed using different parameters (e.g., "off-resonance conditions"), the observed trends may look substantially different. For example, if the B_{HIGH} sweep is performed with τ_{LOW} = 10 ms (versus 6 ms), the P_{13C} maximum is no longer located in the range of 12–22 μT, Figure 3e,b, respectively. Moreover, a τ_{HIGH} sweep performed with τ_{LOW} = 10 ms, Figure 3f (versus 6 ms, Figure 3d) exhibits "spikes" that resemble sinusoidal periodicity, yet the maxima positions remain the same, Figures 3f,d and 4.

The optimal pulsed field conditions are found at τ_{LOW} = 6 ms, B_{LOW} = 0 μT, τ_{HIGH} = 96 μs, and B_{HIGH} = −28 μT. Under these conditions, the P_{13C} build-up rate and final polarization are equivalent to the optimal continuous field experiment at B = −0.42 μT as in Figure 5a. Furthermore, and perhaps more surprisingly, Figure 5b shows that the polarization decay after hyperpolarization is also identical when the sample is exposed to these field conditions. For these experiments, once P_{13C} was fully established in our sample, the pH_2 flow was stopped, the sample was allowed to depolarize at the field of interest, and P_{13C} was then checked using a 1.4 T NMR spectrometer. Systematic mapping of this process allows measuring effective ^{13}C polarization decay rates at arbitrary fields of interest. These mono-exponential decay constants in Figure 5c were measured for fields ranging from 0.21 μT down to 0 μT, showing a sharp decrease as the field approaches 0 μT: 1.9 ± 0.9 s (at 0.00 ± 0.04 μT), 5.8 ± 0.9 s (at −0.06 μT), 9.6 ± 0.7 s (at −0.11 μT), and 20.7 ± 0.3 s (at −0.21 μT). We have also performed simulations using a model of a normal distribution for the field inhomogeneity centered about some average field (5, 10, 20, 40, 80, and 160 nT, Figure 5e) with a standard deviation that is equal to half the average field. This simplistic model clearly shows that as the residual B_{x-y} field increases, T_d decreases even at relatively high Bz values of 0.42 μT, Figure 5e. Qualitative inspection of these simulated trends with experimental data (black trace in Figure 5e) and quantitative RMSD analysis (Figure 5f) reveal the magnitude of residual B_{x-y} field of approximately 80 nT. This value is in overall good agreement with an estimated residual field of 40 nT (in each direction, i.e., B_x and B_y) combined with the precision of our measurement device. The polarization decay was also measured at Earth's field to approximate the behavior under B_{HIGH}, and at the measurement field, 1.4 T in Figure 5d. These decay constants—26.4 ± 1.2 and 79.3 ± 1.9 s, respectively—were "predictably" longer than the corresponding near-zero measurements. Previous ^{15}N SABRE-SHEATH studies with the IrIMes catalyst[40,41] revealed efficient T_1 relaxation in microtesla magnetic fields, which has been rationalized through the substrate's exchange with the catalyst, acting as a source of relaxation for the nearby spins due to different potential contributions (including enhanced scalar relaxation of the second kind—i.e., from interactions with quadrupolar Ir[42,43]—and/or contributions from the exchange itself).

As the relaxation rate is dependent on the correlation time for a specific molecule (on the order of picoseconds), the instantaneous field in the proposed sequence will govern the relaxation dynamics. One would therefore expect that the polarization decay rate for the pulsed field experiments, which stays at 0 μT for ∼98% of the total field sequence duration, would be similar to the decay rate for the 0 μT static field. However, we see a marked decrease in the polarization decay for the static 0 μT field condition.

These dramatic changes in apparent relaxation dynamics at near-zero field should not be mistakenly taken for ^{13}C T_1 decrease because the spin system of interest does not experience any new energy level crossing that may potentially result in additional sources of spin relaxation; instead, we rationalize these observations through the existence of weak residual magnetic fields in the $x-y$ plane (arising from the Earth and/or magnetization of the shield), which are orthogonal to the B_0 field supplied by the solenoid magnet along the z-axis, Figure 1d. As a result, ^{13}C polarization rapidly dephases at an ever-increasing pace as the B_0 decreases in our

https://doi.org/10.1021/acs.jpca.2c07150
J. Phys. Chem. A XXXX, XXX, XXX−XXX

experiment, shown in Figure 5c, resulting in a ^{13}C effective depolarization constant, T_d, that becomes progressively smaller compared to T_1 as measured at B_z of −0.42 μT or at the Earth's magnetic field (*ca.* 50 μT), as B_z approaches 0 μT. On the other hand, during a pulsed experiment, the sample experiences near-zero field dephasing for a negligible period of time compared to $1/\omega_0$ (e.g., at 0.04 μT residual x−y field, $1/\omega_0$ is ∼2 s, which is vastly greater than the 6 ms duration employed in Figure 5a). In other words, the ^{13}C spins dephase by less than 1° during 6 ms at a 0.04 μT dephasing field (estimated by dividing the Earth's magnetic field value of *ca.* 50 μT by the shield attenuation factor of ∼1200). Next, the short application of the −28 μT pulse effectively recovers the dephasing effects of the near-zero x−y residual magnetic fields because, during 96 μs (e.g., Figure 5a), the ^{13}C spin can cover >100°, which is vastly greater than dephasing by 1°. This spin-system behavior becomes possible because $\tau_{LOW}/(1/\omega_0)$ or $\tau_{LOW}\cdot\omega_0$ is substantially lower at B_{LOW} compared to that at B_{HIGH}. These observations are important because the field of SABRE-SHEATH hyperpolarization is rapidly expanding and new cutting-edge approaches are being developed. Since most experimental setups employ multi-layered shields that are similar to those employed in the presented studies, one may potentially overinterpret relaxation dynamics observations such as those shown in Figure 5c. The limitation of such experimental setups (including ours) operating at static magnetic fields (especially for measurements of polarization build-up and decay at B_z approaching 0 μT) can be potentially improved through the implementation of x−y coils and the application of alternating $(+x)$−$(+y)$-$(-x)$−$(-y)$ pulses to decouple the dephasing effects of residual x−y magnetic fields in the shields—examples of such approaches in the context of other applications have been presented previously,[37] and future studies of experimental designs to compensate these effects are certainly warranted.

Overall, the square-microtesla-pulse approach and static-field approach yield overall similar (within experimental error) build-up and relaxation decay rates in the microtesla regime, Figure 5a. The gain in observed ^{13}C polarization (14.8% in this report, Figure 1b) versus ∼12% (in our recent reports[25,26]) in [1-^{13}C]pyruvate is primarily the result of the use of the overall higher p-H_2 pressure and flow rates: 120 sccm at 9.2 atm versus 70 sccm and 8 atm, respectively. These observations suggest that P_{13C} on [1-^{13}C]pyruvate can be further additionally improved through the use of high-pressure and high-flow experimental setups—work in progress in our laboratories. We anticipate that these pilot experimental results will stimulate future theoretical studies of ^{13}C pulsed SABRE-SHEATH in the context of [1-^{13}C]pyruvate and other biologically relevant molecules. Furthermore, we speculate that more robust and efficient pulsed approaches may be possible to further boost [1-^{13}C]pyruvate polarization efficiency via SABRE-SHEATH by minimizing the sample exposure to near-zero magnetic fields to reduce the contribution from unfavorable relaxation. From the substrate perspective, we foresee the immediate application of the presented approach to other bio-α-ketocarboxylates including [1-^{13}C]α-ketoglutarate[44] and [1-^{13}C]α-ketoisocaproate.[45]

CONCLUSIONS

We have reported on the utility of the pulsed SABRE-SHEATH approach to efficiently hyperpolarize ^{13}C nucleus to yield P_{13C} of nearly 15% at the time of detection. The P_{13C} of the pulsed approach matches that of the static SABRE-SHEATH performed at the optimum field of −0.42 μT despite vastly unfavorable P_{13C} dephasing dynamics at the near-zero magnetic field, where the spin system spends most of its time during the pulsed experiment. Importantly, in the context of biomedical translation, the presented results were obtained at a relatively high [1-^{13}C]pyruvate concentration of 27 mM in 0.6 mL volume, which would provide a sufficient bolus for future pilot *in vivo* applications of HP [1-^{13}C]pyruvate produced via SABRE-SHEATH in small rodents. Although HP [1-^{13}C]-pyruvate was prepared here in CD_3OD with 6 mM IrIMes catalyst, the recent advances in the SABRE-catalyst removal[46−48] and HP substrate reconstitution in biocompatible media[49] bode well for near-future biomedical translation of HP [1-^{13}C]pyruvate produced via pulsed SABRE-SHEATH—a subject of ongoing efforts in our partnering laboratories.

AUTHOR INFORMATION

Corresponding Author

Eduard Y. Chekmenev − *Department of Chemistry, Integrative Biosciences (IBio), Karmanos Cancer Institute (KCI), Wayne State University, Detroit, Michigan 48202, United States; Russian Academy of Sciences, Moscow 119991, Russia;* orcid.org/0000-0002-8745-8801; Email: chekmenevlab@gmail.com

Authors

Shiraz Nantogma − *Department of Chemistry, Integrative Biosciences (IBio), Karmanos Cancer Institute (KCI), Wayne State University, Detroit, Michigan 48202, United States*

Shannon L. Eriksson − *Department of Chemistry and School of Medicine, Duke University, Durham, North Carolina 27708, United States*

Isaiah Adelabu − *Department of Chemistry, Integrative Biosciences (IBio), Karmanos Cancer Institute (KCI), Wayne State University, Detroit, Michigan 48202, United States*

Iuliia Mandzhieva − *Department of Chemistry, North Carolina State University, Raleigh, North Carolina 27695-8204, United States*

Austin Browning − *Department of Chemistry, North Carolina State University, Raleigh, North Carolina 27695-8204, United States*

Patrick TomHon − *Department of Chemistry, North Carolina State University, Raleigh, North Carolina 27695-8204, United States;* orcid.org/0000-0003-3202-9812

Warren S. Warren − *Department of Chemistry, Biomedical Engineering, and Radiology, School of Medicine, and Department of Physics, Duke University, Durham, North Carolina 27708, United States;* orcid.org/0000-0001-8458-2076

Thomas Theis − *Department of Chemistry, North Carolina State University, Raleigh, North Carolina 27695-8204, United States;* orcid.org/0000-0001-6779-9978

Boyd M. Goodson − *School of Chemical & Biomolecular Sciences and Materials Technology Center, Southern Illinois University, Carbondale, Illinois 62901, United States;* orcid.org/0000-0001-6079-5077

Complete contact information is available at: https://pubs.acs.org/10.1021/acs.jpca.2c07150

Notes

The authors declare the following competing financial interest(s): Thomas Theis holds stock in Vizma Life Sciences

https://doi.org/10.1021/acs.jpca.2c07150
J. Phys. Chem. A XXXX, XXX, XXX−XXX

LLC (VLS) and is president of VLS. EYC and BMG disclose a stake of ownership in XeUS Technologies, LTD. EYC serves on the Scientific Advisory Board (SAB) of VLS.

■ ACKNOWLEDGMENTS

This work was supported by the National Science Foundation under grants CHE-1904780, CHE-1905341, CHE-2003109, and CHE-1836308, and the National Institute of Biomedical Imaging and Bioengineering of the National Institutes of Health under awards NIH R21EB025313 and NIH R01EB029829. The content is solely the responsibility of the authors and does not necessarily represent the official views of the National Institutes of Health. S.N. and E.Y.C. thank Wayne State University Thomas C. Rumble University Graduate Fellowship.

■ REFERENCES

(1) Nikolaou, P.; Goodson, B. M.; Chekmenev, E. Y. NMR hyperpolarization techniques for biomedicine. *Chem. - Eur. J.* **2015**, *21*, 3156−3166.
(2) Ardenkjær-Larsen, J. H.; Fridlund, B.; Gram, A.; Hansson, G.; Hansson, L.; Lerche, M. H.; Servin, R.; Thaning, M.; Golman, K. Increase in signal-to-noise ratio of >10,000 times in liquid-state NMR. *Proc. Natl. Acad. Sci. U.S.A.* **2003**, *100*, 10158−10163.
(3) Kurhanewicz, J.; Vigneron, D. B.; Brindle, K.; Chekmenev, E. Y.; Comment, A.; Cunningham, C. H.; DeBerardinis, R. J.; Green, G. G.; Leach, M. O.; Rajan, S. S.; et al. Analysis of cancer metabolism by imaging hyperpolarized nuclei: Prospects for translation to clinical research. *Neoplasia* **2011**, *13*, 81−97.
(4) Witte, C.; Schroder, L.; et al. NMR of hyperpolarised probes. *NMR Biomed.* **2013**, *26*, 788−802.
(5) Wang, Y.; Dmochowski, I. J. An expanded palette of xenon-129 NMR biosensors. *Acc. Chem. Res.* **2016**, *49*, 2179−2187.
(6) Eills, J.; Budker, D.; Cavagnero, S.; Chekmenev, E. Y.; Elliott, S. J.; Jannin, S.; Lesage, A.; Matysik, J.; Meersmann, T.; Prisner, T.; Reimer, J. A.; Yang, H.; Koptyug, I. V. Spin hyperpolarization in modern magnetic resonance. *ChemRxiv* **2022**, DOI: 10.26434/chemrxiv-2022-p7c9r.
(7) Golman, K.; in't Zandt, R.; Thaning, M. Real-time metabolic imaging. *Proc. Natl. Acad. Sci. U.S.A.* **2006**, *103*, 11270−11275.
(8) Day, S. E.; Kettunen, M. I.; Gallagher, F. A.; Hu, D. E.; Lerche, M.; Wolber, J.; Golman, K.; Ardenkjaer-Larsen, J. H.; Brindle, K. M. Detecting tumor response to treatment using hyperpolarized C-13 magnetic resonance imaging and spectroscopy. *Nat. Med.* **2007**, *13*, 1382−1387.
(9) Merritt, M.; Harrison, C.; Storey, C.; Jeffrey, F.; Sherry, A.; Malloy, C. Hyperpolarized C-13 allows a direct measure of flux through a single enzyme-catalyzed step by NMR. *Proc. Natl. Acad. Sci. U.S.A.* **2007**, *104*, 19773−19777.
(10) Golman, K.; Axelsson, O.; Johannesson, H.; Mansson, S.; Olofsson, C.; Petersson, J. S. Parahydrogen-induced polarization in imaging: Subsecond C-13 angiography. *Magn. Reson. Med.* **2001**, *46*, 1−5.
(11) Kurhanewicz, J.; Vigneron, D. B.; Ardenkjaer-Larsen, J. H.; Bankson, J. A.; Brindle, K.; Cunningham, C. H.; Gallagher, F. A.; Keshari, K. R.; Kjaer, A.; Laustsen, C.; et al. Hyperpolarized ^{13}C MRI: Path to clinical translation in oncology. *Neoplasia* **2019**, *21*, 1−16.
(12) Brindle, K. M.; Bohndiek, S. E.; Gallagher, F. A.; Kettunen, M. I. Tumor imaging using hyperpolarized C-13 magnetic resonance. *Magn. Reson. Med.* **2011**, *66*, 505−519.
(13) Gatenby, R. A.; Gillies, R. J. Why do cancers have high aerobic glycolysis? *Nat. Rev. Cancer* **2004**, *4*, 891−899.
(14) Ardenkjaer-Larsen, J. H. On the present and future of dissolution-DNP. *J. Magn. Reson.* **2016**, *264*, 3−12.
(15) Kovtunov, K. V.; Pokochueva, E. V.; Salnikov, O. G.; Cousin, S.; Kurzbach, D.; Vuichoud, B.; Jannin, S.; Chekmenev, E. Y.; Goodson, B. M.; Barskiy, D. A.; et al. Hyperpolarized NMR: D-DNP, PHIP, and SABRE. *Chem. - Asian J.* **2018**, *13*, 1857−1871.
(16) Federspiel, M.; Stahr, K.; Hansen, A.; Højgaard, L.; Kjar, A. Production of hyperpolarized ^{13}C-pyruvate by dissolution dynamic nuclear polarization. *J. Nucl. Med.* **2016**, *57*, 2639.
(17) Bowers, C. R.; Weitekamp, D. P. Transformation of symmetrization order to nuclear-spin magnetization by chemical-reaction and nuclear-magnetic-resonance. *Phys. Rev. Lett.* **1986**, *57*, 2645−2648.
(18) Adams, R. W.; Aguilar, J. A.; Atkinson, K. D.; Cowley, M. J.; Elliott, P. I. P.; Duckett, S. B.; Green, G. G. R.; Khazal, I. G.; Lopez-Serrano, J.; Williamson, D. C. Reversible interactions with para-hydrogen enhance NMR sensitivity by polarization transfer. *Science* **2009**, *323*, 1708−1711.
(19) Adams, R. W.; Duckett, S. B.; Green, R. A.; Williamson, D. C.; Green, G. G. R. A theoretical basis for spontaneous polarization transfer in non-hydrogenative parahydrogen-induced polarization. *J. Chem. Phys.* **2009**, *131*, No. 194505.
(20) Theis, T.; Truong, M. L.; Coffey, A. M.; Shchepin, R. V.; Waddell, K. W.; Shi, F.; Goodson, B. M.; Warren, W. S.; Chekmenev, E. Y. Microtesla SABRE enables 10% nitrogen-15 nuclear spin polarization. *J. Am. Chem. Soc.* **2015**, *137*, 1404−1407.
(21) Truong, M. L.; Theis, T.; Coffey, A. M.; Shchepin, R. V.; Waddell, K. W.; Shi, F.; Goodson, B. M.; Warren, W. S.; Chekmenev, E. Y. ^{15}N hyperpolarization by reversible exchange using SABRE-SHEATH. *J. Phys. Chem. C* **2015**, *119*, 8786−8797.
(22) Barskiy, D. A.; Shchepin, R. V.; Tanner, C. P. N.; Colell, J. F. P.; Goodson, B. M.; Theis, T.; Warren, W. S.; Chekmenev, E. Y. The absence of quadrupolar nuclei facilitates efficient ^{13}C hyperpolarization via reversible exchange with parahydrogen. *ChemPhysChem* **2017**, *18*, 1493−1498.
(23) Iali, W.; Roy, S. S.; Tickner, B. J.; Ahwal, F.; Kennerley, A. J.; Duckett, S. B. Hyperpolarising pyruvate through signal amplification by reversible exchange (SABRE). *Angew. Chem., Int. Ed.* **2019**, *58*, 10271−10275.
(24) Tickner, B. J.; Semenova, O.; Iali, W.; Rayner, P. J.; Whitwood, A. C.; Duckett, S. B. Optimisation of pyruvate hyperpolarisation using SABRE by tuning the active magnetisation transfer catalyst. *Catal. Sci. Technol.* **2020**, *10*, 1343−1355.
(25) Adelabu, I.; TomHon, P.; Kabir, M. S. H.; Nantogma, S.; Abdulmojeed, M.; Mandzhieva, I.; Ettedgui, J.; Swenson, R. E.; Krishna, M. C.; Theis, T.; et al. Order-unity ^{13}C nuclear polarization of [1-^{13}C]pyruvate in seconds and the interplay of water and SABRE enhancement. *ChemPhysChem* **2022**, *23*, 131−136.
(26) TomHon, P.; Abdulmojeed, M.; Adelabu, I.; Nantogma, S.; Kabir, M. S. H.; Lehmkuhl, S.; Chekmenev, E. Y.; Theis, T. Temperature cycling enables efficient ^{13}C SABRE-SHEATH hyperpolarization and imaging of [1-^{13}C]-pyruvate. *J. Am. Chem. Soc.* **2022**, *144*, 282−287.
(27) Chapman, B.; Joalland, B.; Meersman, C.; Ettedgui, J.; Swenson, R. E.; Krishna, M. C.; Nikolaou, P.; Kovtunov, K. V.; Salnikov, O. G.; Koptyug, I. V.; et al. Low-cost high-pressure clinical-scale 50% parahydrogen generator using liquid nitrogen at 77 K. *Anal. Chem.* **2021**, *93*, 8476−8483.
(28) Cavallari, E.; Carrera, C.; Sorge, M.; Bonne, G.; Muchir, A.; Aime, S.; Reineri, F. The ^{13}C hyperpolarized pyruvate generated by parahydrogen detects the response of the heart to altered metabolism in real time. *Sci. Rep.* **2018**, *8*, No. 8366.
(29) Hövener, J.; Pravdivtsev, A. N.; Kidd, B.; Bowers, C. R.; Glöggler, S.; Kovtunov, K. V.; Plaumann, M.; Katz-Brull, R.; Buckenmaier, K.; Jerschow, A.; et al. Parahydrogen-based hyperpolarization for biomedicine. *Angew. Chem., Int. Ed.* **2018**, *57*, 11140−11162.
(30) Lindale, J. R.; Eriksson, S. L.; Tanner, C. P. N.; Zhou, Z.; Colell, J. F. P.; Zhang, G.; Bae, J.; Chekmenev, E. Y.; Theis, T.; Warren, W. S. Unveiling coherently driven hyperpolarization dynamics in signal amplification by reversible exchange. *Nat. Commun.* **2019**, *10*, No. 395.

(31) Tanner, C. P. N.; Lindale, J. R.; Eriksson, S. L.; Zhou, Z.; Colell, J. F. P.; Theis, T.; Warren, W. S. Selective hyperpolarization of heteronuclear singlet states via pulsed microtesla SABRE. *J. Chem. Phys.* **2019**, *151*, No. 044201.
(32) Dagys, L.; Bengs, C.; Levitt, M. H. Low-frequency excitation of singlet−triplet transitions. Application to nuclear hyperpolarization. *J. Chem. Phys.* **2021**, *155*, No. 154201.
(33) Eriksson, S. L.; Lindale, J. R.; Li, X.; Warren, W. S. Improving SABRE hyperpolarization with highly nonintuitive pulse sequences: Moving beyond avoided crossings to describe dynamics. *Sci. Adv.* **2022**, *8*, No. eabl3708.
(34) Pravdivtsev, A. N.; Kempf, N.; Plaumann, M.; Bernarding, J.; Scheffler, K.; Hövener, J.-B.; Buckenmaier, K. Coherent evolution of signal amplification by reversible exchange in two alternating fields (alt-SABRE). *ChemPhysChem* **2021**, *22*, 2381−2386.
(35) Cowley, M. J.; Adams, R. W.; Atkinson, K. D.; Cockett, M. C. R.; Duckett, S. B.; Green, G. G. R.; Lohman, J. A. B.; Kerssebaum, R.; Kilgour, D.; Mewis, R. E. Iridium N-heterocyclic carbene complexes as efficient catalysts for magnetization transfer from para-hydrogen. *J. Am. Chem. Soc.* **2011**, *133*, 6134−6137.
(36) Vazquez-Serrano, L. D.; Owens, B. T.; Buriak, J. M. The search for new hydrogenation catalyst motifs based on N-heterocyclic carbene ligands. *Inorg. Chim. Acta* **2006**, *359*, 2786−2797.
(37) Nantogma, S.; Joalland, B.; Wilkens, K.; Chekmenev, E. Y. Clinical-scale production of nearly pure (>98.5%) parahydrogen and quantification by benchtop NMR spectroscopy. *Anal. Chem.* **2021**, *93*, 3594−3601.
(38) Barskiy, D. A.; Kovtunov, K. V.; Koptyug, I. V.; He, P.; Groome, K. A.; Best, Q. A.; Shi, F.; Goodson, B. M.; Shchepin, R. V.; Coffey, A. M.; et al. The feasibility of formation and kinetics of NMR signal amplification by reversible exchange (SABRE) at high magnetic field (9.4 T). *J. Am. Chem. Soc.* **2014**, *136*, 3322−3325.
(39) Joalland, B.; Nantogma, S.; Chowdhury, M. R. H.; Nikolaou, P.; Chekmenev, E. Y. Magnetic shielding of parahydrogen hyperpolarization experiments for the masses. *Magn. Reson. Chem.* **2021**, *59*, 1180−1186.
(40) Birchall, J. R.; Kabir, M. S. H.; Salnikov, O. G.; Chukanov, N. V.; Svyatova, A.; Kovtunov, K. V.; Koptyug, I. V.; Gelovani, J. G.; Goodson, B. M.; Pham, W.; Chekmenev, E. Y. Quantifying the effects of quadrupolar sinks via ^{15}N relaxation dynamics in metronidazoles hyperpolarized via SABRE-SHEATH. *Chem. Commun.* **2020**, *56*, 9098−9101.
(41) Shchepin, R. V.; Jaigirdar, L.; Chekmenev, E. Y. Spin-lattice relaxation of hyperpolarized metronidazole in signal amplification by reversible exchange in micro-tesla fields. *J. Phys. Chem. C* **2018**, *122*, 4984−4996.
(42) Blanchard, J. W.; Sjolander, T. F.; King, J. P.; Ledbetter, M. P.; Levine, E. H.; Bajaj, V. S.; Budker, D.; Pines, A. Measurement of untruncated nuclear spin interactions via zero- to ultralow-field nuclear magnetic resonance. *Phys. Rev. B* **2015**, *92*, No. 220202.
(43) Bernatowicz, P.; Kubica, D.; Ociepa, M.; Wodyński, A.; Gryff-Keller, A. Scalar relaxation of the second kind. A potential source of information on the dynamics of molecular movements. 4. Molecules with collinear C−H and C−Br bonds. *J. Phys. Chem. A* **2014**, *118*, 4063−4070.
(44) Adelabu, I.; Ettedgui, J.; Joshi, S. M.; Nantogma, S.; Chowdhury, M. R. H.; McBride, S.; Theis, T.; Sabbasani, V. R.; Chandrasekhar, M.; Sail, D.; et al. Rapid ^{13}C hyperpolarization of the TCA cycle intermediate α-ketoglutarate via SABRE-SHEATH. *Anal. Chem.* **2022**, *94*, 13422−13431.
(45) Tickner, B. J.; Ahwal, F.; Whitwood, A. C.; Duckett, S. B. Reversible hyperpolarization of ketoisocaproate using sulfoxide-containing polarization transfer catalysts. *ChemPhysChem* **2021**, *22*, 13−17.
(46) Kidd, B. E.; Gesiorski, J. L.; Gemeinhardt, M. E.; Shchepin, R. V.; Kovtunov, K. V.; Koptyug, I. V.; Chekmenev, E. Y.; Goodson, B. M. Facile removal of homogeneous SABRE catalysts for purifying hyperpolarized metronidazole, a potential hypoxia sensor. *J. Phys. Chem. C* **2018**, *122*, 16848−16852.
(47) Barskiy, D. A.; Ke, L. A.; Li, X.; Stevenson, V.; Widarman, N.; Zhang, H.; Truxal, A.; Pines, A. Rapid catalyst capture enables metal-free para-hydrogen-based hyperpolarized contrast agents. *J. Phys. Chem. Lett.* **2018**, *9*, 2721−2724.
(48) Iali, W.; Olaru, A.; Green, G.; Duckett, S. Achieving high levels of NMR-hyperpolarization in aqueous media with minimal catalyst contamination using SABRE. *Chem. - Eur. J.* **2017**, *23*, 10491−10495.
(49) Knecht, S.; Blanchard, J. W.; Barskiy, D.; Cavallari, E.; Dagys, L.; Van Dyke, E.; Tsukanov, M.; Bliemel, B.; Münnemann, K.; Aime, S.; et al. Rapid hyperpolarization and purification of the metabolite fumarate in aqueous solution. *Proc. Natl. Acad. Sci. U. S. A.* **2021**, *118*, No. e2025383118.

https://doi.org/10.1021/acs.jpca.2c07150
J. Phys. Chem. A XXXX, XXX, XXX−XXX